Low-Resistive High-Work-Function Gate Electrode for Transparent a-IGZO TFTs

Woo Jae Jang, Myung Keun Lee, Jinhan Yoo, Eungtaek Kim, Dae Young Yang, Junhong Park, Jeong Woo Park, Sang-Hee Ko Park, and Kyung Cheol Choi, *Senior Member, IEEE*

***Abstract*— Highly transparent and low-resistive multilayered gate electrodes, MoO_3/indium–tin oxide (ITO)/Ag/ZnS (MIAZ) playing as the high-work-function layer, the nonreactive interface layer, the lateral conduction layer, and the index-matching layer, respectively, have been investigated for the application to the transparent oxide thin-film transistors (TFTs). The transmittance of the optimized MIAZ electrode is 92.46% and the sheet resistance is 7.77 Ω/□. The top gate InGaZnO TFT with this gate electrode shows the mobility of 11.57 $cm^2/(V \cdot s)$ and positive V_{th} of 0.210 V compared with that with single ITO gate electrode of which V_{th} is –0.086 V.**

***Index Terms*— a-indium–gallium–zinc oxide (IGZO) thin-film transistors (TFTs), threshold voltage control.**

I. Introduction

With the Internet of Things era arriving, the demand for high-resolution displays is also increasing. In addition, numerous transparent displays that can improve the interaction among people or between people and things have been attracting consumers. The aperture ratio, however, is one of the limitations when attempting to increase the resolution of conventional transparent displays [1]. Since thin-film transistors (TFTs) are not transparent, the occupied area of TFTs in each pixel limits the space through which light can emit from the light source. Furthermore, high-resolution displays require a reduced pixel size with an increased number of TFTs. As a result, each pixel must consume more power to emit higher luminescence in high-resolution displays. The high power consumption shortens the lifetime of the devices and limits increases in the resolution [2]. This poses a serious problem of application for mobiles, which have small pixel sizes than TVs. To address this issue, many studies have been actively conducted with concentration on the transparent TFTs.

Transparent electrodes are very important in transparent TFT and display applications. They require low-resistance and high-transparency levels. The indium–tin oxide (ITO) has been widely used in the gate electrodes of transparent oxide TFTs, because it has high transmittance (>90%) and relatively low resistivity ($1–5 \times 10^{-4}$ Ω·cm) [3], [4]. In a high-resolution display, however, the ITO is not a proper choice of materials due to the *RC* delay, followed by the signal distortion that arises when increasing the distance from the power source. As a result, various replacements for ITO have been suggested [5]–[7].

Most oxide TFTs show high stability with a small negative value turn-ON (V_{on}) voltage [8]. The oxide TFTs with small subthreshold slope as well as the slightly negative V_{on} voltage create high current at a zero gate bias. Since controlling the threshold voltage is very important to maximize the circuit performance and minimize the consumption of standby power, many researchers attempt to control the threshold voltage of oxide TFT with a dual-gate or a back-gate process, controlling the oxygen content at the active layer and changing the active thicknesses. However, these approaches resulted in the degradations of the mobility or stability of devices [9], [10].

In this paper, a transparent TFT with a low-resistive, high-transparent, and threshold-voltage-controllable multilayered gate electrode is presented. The results indicate that an indium–gallium–zinc oxide (IGZO)-based TFT with the proposed electrode is suitable for the real transparent display with high resolution.

II. Electrode Structure and Device Fabrication Method

A. Electrode Structure

The electrodes are composed of four layers as shown in Fig. 1(b). The first layer plays as the high-work-function layer to ensure the proper threshold voltage of the TFT. Molybdenum trioxide (MoO_3) of which work function is higher than that of ITO is a good candidate of high-work-function layer. A nonreactive interface layer is stacked upon the first layer in order for the threshold voltage to be affected only by the first layer. ITO forms a nonreactive interface with the MoO_3 [11]. The third layer is the lateral conduction layer to ensure high conductivity. Silver (Ag) has the lowest optical absorption and highest electrical conductivity among all possible materials. Therefore, Ag is used as the

Manuscript received August 11, 2016; revised October 27, 2016 and November 11, 2016; accepted November 17, 2016. Date of publication December 2, 2016; date of current version December 24, 2016. This work was supported in part by the Open Innovation Lab Project from National Nanofab Center and in part by the Nano·Material Technology Development Program through the National Research Foundation of Korea Funded by the Ministry of Science, ICT and Future Planning under Grant NRF-2016M3A7B4910635. The review of this paper was arranged by Editor R. M. Todi.

W. J. Jang, M. K. Lee, J. Yoo, E. Kim, D. Y. Yang, J. Park, J. W. Park, and K. C. Choi are with the School of Electrical Engineering, Korea Advanced Institute of Science and Technology, Daejeon 305-701, South Korea (e-mail: kyungcc@kaist.ac.kr).

S.-H. K. Park is with the Department of Materials Science and Engineering, Korea Advanced Institute of Science and Technology, Daejeon 305-701, South Korea (e-mail: shkp@kaist.ac.kr).

Color versions of one or more of the figures in this paper are available online at http://ieeexplore.ieee.org.

Digital Object Identifier 10.1109/TED.2016.2631567

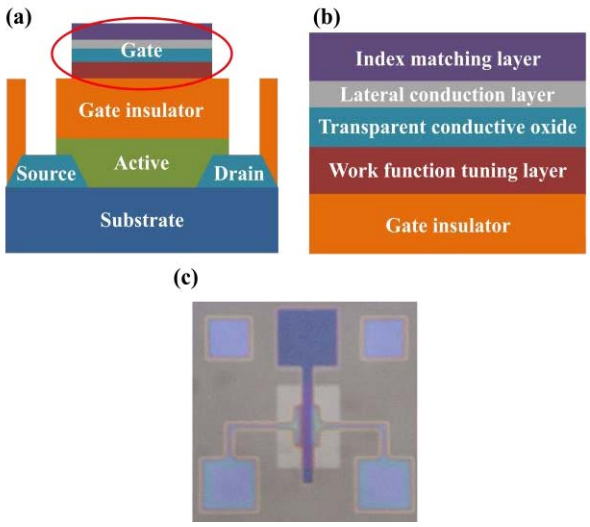

Fig. 1. (a) Schematic cross section of a top gate bottom contact TFT. (b) Schematic cross section of a gate electrode in red circle at (a). (c) Photomicrograph of TFT.

lateral conduction layer [12], [13]. The final top layer is the index-matching layer. When an electrode includes a thin metal layer, it has low transmittance because of not the absorption but the reflection of the metal [12]. Consequently, we can enhance the electrode transmittance by reducing the reflection with destructive interference. Therefore, zinc sulfide (ZnS) is used thanks to its high refractive index in the index-matching layer. The final structure of the gate electrode is designed to be MoO_3/ITO/Ag/ZnS (MIAZ).

B. Device Fabrication

Here a top-gate bottom-contact TFT structure was used. Before device fabrication, tooling factor calculation was conducted to accurately control the thermal evaporator deposition process. A schematic of the cross-section and a photomicrograph of the TFT are shown in Fig. 1(a) and (c), respectively. The device length (L) and width (W) were 70.5 and 473 μm, respectively. It was possible to minimize the device size using the lift-off patterning process to fabricate device with a channel length of a few micrometers, which is a requirement for the current state-of-the-art pixel size [14]. The fabrication process sequence is as follows. First, a 150-nm-thick ITO film on 700-μm-thick nonalkali glass substrate was cleaned using acetone, isopropyl alcohol, and deionized water in sequence in a sonication bath. In order to form the ITO source and drain pattern, the conventional photolithography process was used. The etching process was performed by a wet process using a mixed etchant solution of MA-SO2 (HCl:HNO_3-based acid solution, Dongwoo Fine-Chem.) for 15 s. After patterning the source and drain electrode, 20-nm-thick 1:1:1 IGZO was deposited by sputtering. The Ar:O_2 ratio was 48:2 during the sputtering step, and 9-nm-thick aluminum oxide (Al_2O_3) was deposited by means of thermal ALD to protect the active-gate insulator interface. The Al_2O_3 thickness was controlled by the process cycle number. In order to define the IGZO active layer, the patterning process was done by wet etching process with diluted HF. Subsequently, 350 °C annealing was conducted for 3 h and 30 min in a furnace, after which a 31-nm additional Al_2O_3 layer was deposited to form the gate insulator. Postannealing has been conducted for 2 h in a furnace at 350 °C. For the contact to the source and drain ITO electrode, vias were formed using a wet etching process at 120 °C with phosphoric acid (H3PO4). Both gate electrodes, ITO and the newly designed multilayered electrode, were formed with a shadow mask. In the case of the MIAZ gate electrode, first, to maximize the MoO3 purity, MoO3 was deposited using a thermal evaporator under an internal pressure below 2e-5 (torr), with the deposition speed maintained at 0.5 Å/s for accurate thickness control. After ITO deposition, followed by thermal annealing at 400 °C, Ag and ZnS were sequentially deposited.

III. Optimization of Electrode

The optimization of electrode structure was conducted with the consideration of the electrical and optical characteristics of the TFT. The threshold voltage of the TFT was determined by the constant current method considering the geometrical factors of the device. The threshold voltage (V_{th}) was determined using the value of V_{gs}, which induced an Ids of $W/L \times 10$ nA at a V_{ds} of 0.1 V. The saturation mobility was determined from the equations shown below. The work function of the MoO3 and the ITO were extracted using the EFM peak amplitude difference with Graphite (4.56 eV) [15]

$$\sqrt{I_{ds}} = \sqrt{\frac{W}{2L}\mu_{sat}C_{ox}}(V_{gs} - Vt)$$

$$\text{Slope} = \sqrt{\frac{W}{2L}\mu_{sat}C_{ox}}$$

$$\mu_{sat} = \text{Slope}^2 / \left(\frac{W}{2L} \cdot C_{ox}\right).$$

The transmittance of the nonpatterned gate electrode film was measured using a UV-VIS spectrophotometer (UV-2550, SHIMADZU) in a wave length range from 380 to 720 nm, with automatic normalizing of the transmittance of the 700-μm thick soda lime glass.

A. High-Work-Function Layer

MoO_3 was used as a high-work-function layer to ensure the proper threshold voltage. However, the conductivity of MoO_3 proved not to be ideal for a gate electrode. Use of low conductive electrode layer increases the parasitic capacitance, which can degrade display performance. Therefore, it was necessary to optimize the MoO_3 thickness to yield threshold voltage shift without degradation of the device performance. Fig. 2(a) shows the linear-scale transfer curve distribution with the same MoO3 thickness within the range of 5 to 40 nm. The values of the mobility distribution are summarized in Table I. Eventually, 5 nm of MoO_3 was chosen, because the hysteresis of TFT was smaller at that thickness, as shown in the inset of Fig. 2(b). Fig. 3 shows the transfer curves of TFTs with ITO and the MoO_3 gate electrode as the reference and tested TFT, respectively. The mobility and gate work function are presented in Table II. The work function of the gate electrode was measured by means of scanning Kelvin-probe microscopy (Xe-70 made by Park Systems). As previously reported,

TABLE I

Mobility According to Thicknesses of MoO_3 at MIAZ Structure

	MoO_3 thickness (nm)	μ_{sat} ($cm^2/(V{\cdot}s)$)
IGZO / Al_2O_3 / MoO_3(x) / ITO	5	10.86 (± 0.255)
	10	11.32 (± 0.235)
	15	9.48 (± 0.34)
	20	8.4 (± 0.32)
	25	8.86 (± 0.535)

TABLE II

Mobility and Work Function of TFTs

	ITO	MIAZ
Work function (eV)	4.75	4.97
μ_{sat}($cm^2/(V{\cdot}s)$)	11.46	11.84

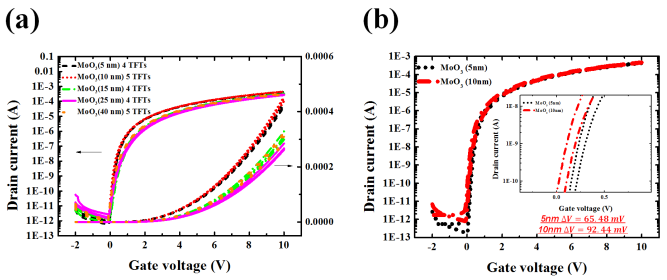

Fig. 2. V_{ds} was 10 V. (a) Transfer curves with changing the MoO_3 thickness from 5 to 40 nm. (b) Transfer curves of 5- and 10-nm MoO_3. Inset of (b) hysteresis of transfer curve at (b).

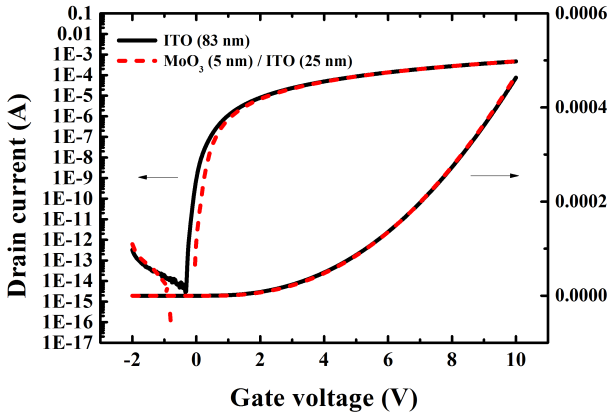

Fig. 3. V_{ds} was 10 V. Transfer curves of ITO gate and MoO_3 5-nm gate.

the work function of MoO_3 is higher than that of ITO [16], [17]. It was confirmed that the TFT offers similar mobility with either the ITO or the MoO_3 gate.

B. Non-Reactive Interface Layer

The ITO was used as a nonreactive interface layer [11]. The ITO thickness was designed to maximize the optical and electrical properties of the TFT. As shown in Fig. 4(b), according to the results of the optical simulation of the red square region of TFT in Fig. 4(a), the change of the thickness of ZnS induces dramatic change of the device transmittance. Meanwhile, the change of thickness of the ITO scarcely affects

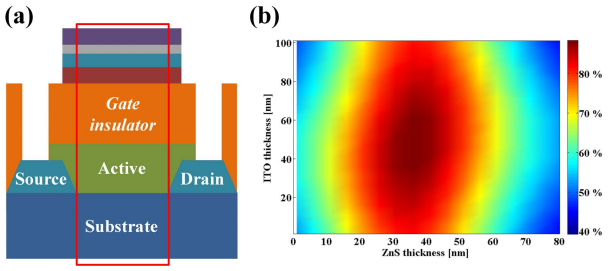

Fig. 4. (a) Describing the simulation region by red square. (b) Luminous transmittance simulation results of red square region in (a).

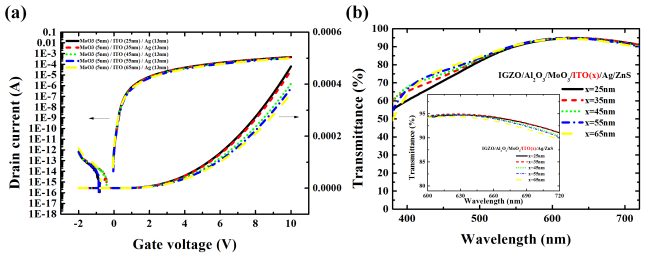

Fig. 5. V_{ds} was 10 V. (a) Transfer curves of MoO_3(5 nm)/ITO(x nm)/Ag (13 nm) gate with varying ITO thickness. (b) Spectral transmittance of IGZO(20 nm)/Al_2O_3 (40 nm)/MoO_3 (5 nm)/ITO (x nm)/Ag (13 nm)/ZnS (35 nm) with varying ITO thickness. Inset of (b) expanding long wavelength region of (b). *x* value: 25, 35, 45, 55, and 65 nm.

TABLE III

Mobility and Luminous Transmittance With Thickness of ITO and MIAZ Structure

ITO thickness (nm)	25	35	45	55	65
μ_{sat} ($cm^2/(V{\cdot}s)$)	11.84	11.46	10.27	10.09	9.48
Luminous transmittance (%)	89.98	90.58	90.48	90.73	90.74

the TFT transmittance. Therefore, the electrical properties were investigated prior to the optical properties. Fig. 5(a) and Table III show the performance of TFT depending on the ITO thickness from 25 to 65 nm. It was found that when the ITO thickness exceeded 35 nm, the TFT mobility was reduced. Therefore, the ITO thickness was set to less than 35 nm considering the device mobility. The spectral transmittances of the MIAZ electrodes are shown in Fig. 5(b). Contrary to our expectation which the transmittance results would be similar regardless of changing thickness of the ITO, the spectral transmittance of the IGZO/PL layers with MIAZ electrode was observed to exhibit red shift of peak transmittance greater than 550 nm. As shown in the inset in Fig. 5(b), when the ITO thickness was 35 nm, the MIAZ electrode attained the highest transmittance in the long wavelength range. To improve the transmittance of MIAZ electrode, the adjustment of ZnS thickness, inducing blue shift of the peak wavelength, is necessary. Consequently, the ITO thickness was fixed at 35 nm and ZnS thickness was optimized as described in Section III-D.

C. Lateral Conduction Layer

Although Ag is well-known electrode with high conductivity, the formation of very thin Ag layer for

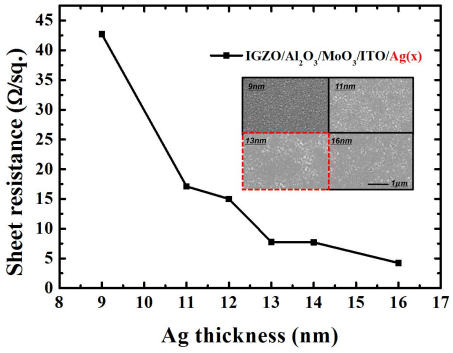

Fig. 6. Sheet resistance with Ag thickness increasing. Inset: SEM images of Ag surface morphology deposited on ITO film.

the transparent electrode mostly yields island clusters with thickness below the critical thickness [13], [18]–[20], resulting in high sheet resistance due to disconnections between the Ag clusters [12], [13]. Fig. 6 shows a sheet resistance of MIAZ films according to the thickness of Ag films. When the thickness of Ag is 13 nm, the slope of resistance is greatly reduced, suggesting that Ag should form a conductive film at 13 nm. The sheet resistance of Ag at 13 nm was 7.77 Ω/□. The scanning electron microscopies of Ag film surfaces are shown in the inset of Fig. 6 to support this result. Increasing Ag thickness beyond 13 nm made no remarkable differences in sheet resistance. Furthermore, increased light absorption from the Ag films thicker than 13 nm limits the Ag thickness to 13 nm for optimization.

D. Index Matching Layer

The ZnS was used as an index-matching layer [13], [21], [22]. As described previously in Fig. 4(b), the device transmittance is remarkably influenced by changing the thickness of the ZnS. In order to enhance the film transmittance, the reflected light from the Ag layer was reduced by means of destructive interference. In order to realize destructive interference at the index-matching layer, the phase difference should be 180 between the reflections of lights, and the two beams must have the same amplitude. Therefore, it was concluded that when ZnS thickness was determined by equation shown, destructive interference occurred at a specific wavelength

$$nd = \frac{\lambda}{4}.$$

The symbols n, d, and λ are the refractive index, the thickness of the index-matching layer, and the wavelength of light, respectively. The experiment involved changing the ZnS thickness from 20 to 40 nm at 5 nm intervals on the basis of the simulation results shown in Fig. 4(b). As shown in Fig. 7 and Table IV, the reduction of thickness of ZnS resulted in blue shift of the peak wavelength in accordance with equation shown before. When the ZnS thickness was 30 nm, the device had the highest luminous transmittance of 92.46%. Consequently, the ZnS thickness was fixed at 30 nm. Finally, the device was optimized with 5 nm of MoO_3 as the high-work-function layer, 35 nm of ITO as the nonreactive interface layer, 13 nm of Ag as the lateral conduction layer,

TABLE IV
Transmittance Characteristics Depending on Thickness of ZnS at MIAZ Structure

ZnS thickness (nm)	20	25	30	35	40
Luminous transmittance (%)	87.01	91.40	92.46	90.58	86.41
Maximum transmittance (%)	89.47	92.94	94.29	94.95	94.31
Peak wavelength (nm)	523	539	577	629	661

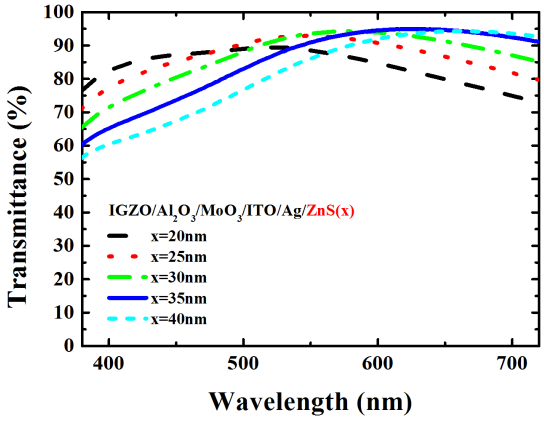

Fig. 7. Spectral transmittance of IGZO/Al_2O_3/MoO_3/ITO/Ag/ZnS(x nm and x = 20, 25, 30, 35, and 40).

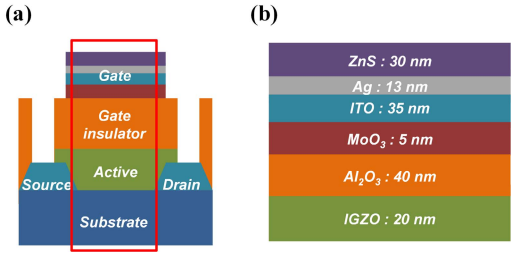

Fig. 8. (a) Describing the whole structure. (b) Optimized structure with each thickness for materials.

and 30 nm of ZnS as the index-matching layer. Fig. 8 presents this structure.

IV. Results and Discussion

A. Electrode Performance

To assess the performance of the optimized electrode, the ITO electrode was fabricated on an IGZO (20 nm)/Al_2O_3 (40 nm) film. The thickness of ITO is 83 nm, which is the same as optimized MIAZ electrode. Fig. 9 presents the spectral transmittance of the optimized MIAZ electrode. The inset of Fig. 9 is a photograph of transparent TFTs that were applied to the MIAZ electrode and to the ITO electrode. The MIAZ-electrode TFTs show clear letters and photographs through. Table V shows the properties of the ITO electrode and the MIAZ electrode. The luminous transmittance levels of both ITO and MIAZ were approximately 92%, meaning that they appeared nearly identical. Fig. 9 shows that ITO has higher transmittance both in the long wavelength and in the short wavelength region, whereas the MIAZ had higher transmittance in the 550-nm wavelength region, which can be

TABLE V
Properties of TFTs Using ITO and MIAZ Gate Electrode

	ITO	MIAZ
Luminous transmittance (%)	92.64	92.46
Maximum transmittance (%)	93.12	94.29
Peak wavelength (nm)	599	577
550nm transmittance (%)	92.92	93.52
Sheet resistance (Ω/□)	39.96	7.77
Resistivity (Ω·cm)	3.32×10^{-4}	6.45×10^{-5}
Figure of merit ($10^{-3}\cdot\Omega^{-1}$)	12.01	65.86

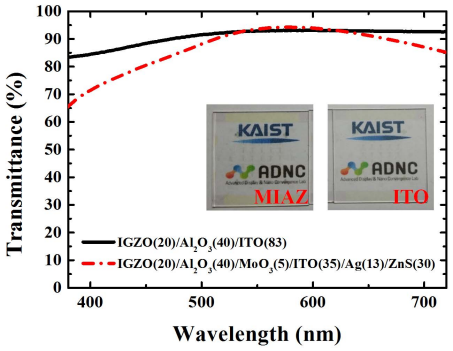

Fig. 9. Spectral transmittance of TFTs when using ITO gate electrode and MIAZ gate electrode. Inset: Photograph of TFTs when using MIAZ and ITO gate electrode.

easily detected by human eyes. Therefore, we can say that the two electrodes have similar luminous transmittance levels in practice. The sheet resistance of the ITO electrode was 39.96 Ω/□ and that of the MIAZ electrode was 7.77 Ω/□, five times lower than that of ITO. This value was converted, indicating that the resistivity of ITO was 3.32×10^{-4} Ω·cm, a good property, though the MIAZ had a lower resistivity of 6.45×10^{-5} Ω·cm. To evaluate the electrical and optical properties of the transparent electrode simultaneously, the figure of merit method was used [23]

$$\text{Figure of merit, } \emptyset_{TC} = \frac{T^{100}_{5500\ \text{nm}}}{R_{\text{sheet resistance}}}[100^{-3}\cdot\Omega^{-3}].$$

The figure of merit is the transmittance at a wavelength of 550 nm to the power of tenth divided by the sheet resistance, as in the above-mentioned formula. The MIAZ electrode has higher transmittance at a wavelength of 550 nm with lower sheet resistance, and the figure of merit of MIAZ is five or more times larger than that of ITO. Therefore, MIAZ is superior to ITO in terms of the properties of a transparent electrode.

B. TFT Performance

We investigated the effect of work function of gate electrode on the performance of the transparent TFTs with the ITO electrode and the MIAZ electrode. Fig. 10 shows the transfer curve of the TFTs. The V_{th} values of TFTs were tuned on the order of the gate work function as shown in Table I. The threshold voltage of the TFT and the difference between the threshold voltage and the work function are presented in Table VI. Fig. 11 shows the results of the comparison of the threshold voltages between ITO and MIAZ. While the

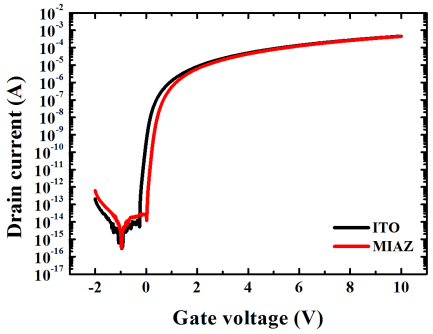

Fig. 10. Transfer curve of TFTs using ITO gate electrode and MIAZ gate electrode.

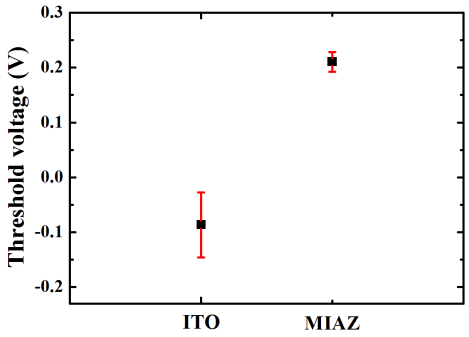

Fig. 11. Threshold voltage of TFTs using ITO and MIAZ gate electrode.

TABLE VI
Threshold Voltage and the Difference Between ITO Gate and MIAZ Gate

	ITO	MIAZ
Average V_{th}	-0.08673	0.21035
ΔV_{th} (V)	0	0.29708
ΔWF (eV)	0	0.22

threshold voltage of ITO was under 0 V, the threshold voltage of MIAZ exceeded 0 V.

The difference in the work function of the TFTs (ΔWF) and the threshold voltage of the TFTs (ΔV_{th}) had to be identical once the interface between the gate and the gate insulator reached an ideal state, meaning that it was defect-free with no pinholes. ΔV_{th}, however, was not identical to ΔWF. It may explain the discord between the effective work function of the gates of actual TFTs and the measured work function of the gates, which has an inverted stack relative to that of an actual gate structure in order to measure the work function. In practice, it is known that the effective work function can vary due to newly generated states, which arise once the gate interface is formed through the chemical reaction between the gate metal and the gate insulator [11]. Thus, the flat-band voltage induced by the measured work function may differ from the flat-band voltage of the fabricated TFTs. Consequently, the final TFTs using MoO_3, which has a higher work function than ITO, showed a turn-ON voltage, which exceeded 0 V and a threshold voltage shift, which matched the tendency of the work-function difference, although the threshold voltage shift was not identical to the difference

TABLE VII
Properties of TFTs Using ITO and MIAZ Gate Electrode

	ITO	MIAZ
Average V_{th}	-0.08673	0.21035
SS (mV/decade)	73.90	70.21
On/off ratio (10^{12})	4.463	1.515
μ_{sat} ($cm^2/(V{\cdot}s)$)	11.42	11.57

between the threshold voltage of the MoO_3 gate and the ITO gate.

Table VII presents the properties of the TFTs. The mobility levels of the TFTs with the ITO gate and the MIAZ gate averaged 11.42 and 11.57 $cm^2/(V \cdot s)$, respectively. The difference in the threshold voltage of the two TFTs averaged 0.297 V. The threshold voltage exceeded 0 V without a decrease in the performance when using the MIAZ gate electrode.

V. Conclusion

In this paper, a gate electrode having better electrical performance as well as similar transmittance to an ITO electrode was investigated. Optimized MIAZ electrode has high conductivity and enables to adjust threshold voltage when applied to the TFT. The threshold voltage of TFT was adjusted using a work-function tuning layer with low sheet resistance realized using a metal (MoO_3) layer. The transmittance of the electrode increased by means of destructive interference.

The luminous transmittance of the optimized MIAZ electrode exceeded 92% with the active layer of the TFT, and the sheet resistance was 7.77 Ω/□. The figure of merit was $65.86 \times 10^{-3} \cdot \Omega^{-1}$. The threshold voltage of the TFT with the MIAZ gate electrode was 0.297 V, which is higher than that of the TFT with the ITO electrode. The change of the threshold voltage is due to the use of MoO_3, which has a higher work function than ITO as a work-function tuning layer. The TFT used with MIAZ showed performance nearly identical to that of ITO, with the control of the threshold voltage.

The transparent TFTs with the low resistive and V_{th} controllable MIAZ electrode make reduce not only the *RC* delay in the TFT array but also stand-by power consumption by adjusting the threshold voltage without degradation of the performance. Furthermore, positive V_{th} of transparent oxide TFT can be applied to transparent logic gates, enable to materialize transparent wearable display such as glass-typed display.

References

[1] E. Kim *et al.*, "Suppressed instability of a-IGZO thin-film transistors under negative bias illumination stress using the distributed Bragg reflectors," *IEEE Trans. Electron Devices*, vol. 63, no. 3, pp. 1066–1071, Mar. 2016.

[2] L. Zhou *et al.*, "Power consumption model for AMOLED display panel based on 2T-1C pixel circuit," *J. Display Technol.*, vol. 12, no. 10, pp. 1064–1069, Oct. 2016.

[3] J. P. Zheng and H. S. Kwok, "Low resistivity indium tin oxide films by pulsed laser deposition," *Appl. Phys. Lett.*, vol. 63, no. 1, pp. 1–3, 1993.

[4] C. Guillén and J. Herrero, "ITO/metal/ITO multilayer structures based on Ag and Cu metal films for high-performance transparent electrodes," *Solar Energy Mater. Solar Cells*, vol. 92, no. 8, pp. 938–941, Aug. 2008.

[5] S. M. Lee, Y. Cho, D. Y. Kim, J. S. Chae, and K. C. Choi, "Enhanced light extraction from mechanically flexible, nanostructured organic light-emitting diodes with plasmonic nanomesh electrodes," *Adv. Opt. Mater.*, vol. 3, no. 9, pp. 1240–1247, 2015.

[6] D. Y. Kim, Y. C. Han, H. C. Kim, E. G. Jeong, and K. C. Choi, "Highly transparent and flexible organic light-emitting diodes with structure optimized for anode/cathode multilayer electrodes," *Adv. Funct. Mater.*, vol. 25, no. 46, pp. 7145–7153, 2015.

[7] S. M. Lee, J. S. Chae, D. Y. Kim, and K. C. Choi, "Plasmonic nanomeshes as large-area, low-resistive transparent electrodes and their application to ITO-free organic light-emitting diodes," *Organic Electron.*, vol. 15, no. 11, pp. 3354–3361, 2014.

[8] H. J. In and O. K. Kwon, "External compensation of nonuniform electrical characteristics of thin-film transistors and degradation of OLED devices in AMOLED displays," *IEEE Electron Device Lett.*, vol. 30, no. 4, pp. 377–379, Apr. 2009.

[9] K. Takechi, M. Nakata, K. Azuma, H. Yamaguchi, and S. Kaneko, "Dual-gate characteristics of amorphous $InGaZnO_4$ thin-film transistors as compared to those of hydrogenated amorphous silicon thin-film transistors," *IEEE Trans. Electron Devices*, vol. 56, no. 9, pp. 2027–2033, Sep. 2009.

[10] M. Mativenga, S. An, and J. Jang, "Bulk accumulation a-IGZO TFT for high current and turn-on voltage uniformity," *IEEE Electron Device Lett.*, vol. 34, no. 12, pp. 1533–1535, Dec. 2013.

[11] M. T. Greiner, L. Chai, M. G. Helander, W.-M. Tang, and Z.-H. Lu, "Metal/metal-oxide interfaces: How metal contacts affect the work function and band structure of MoO_3," *Adv. Funct. Mater.*, vol. 23, no. 2, pp. 215–226, Jan. 2013.

[12] S. Kim and J.-L. Lee, "Design of dielectric/metal/dielectric transparent electrodes for flexible electronics," *J. Photon. Energy*, vol. 2, no. 1, p. 021215, 2012.

[13] D. Y. Yang, S.-M. Lee, W. J. Jang, and K. C. Choi, "Flexible organic light-emitting diodes with ZnS/Ag/ZnO/Ag/WO_3 multilayer electrode as a transparent anode," *Organic Electron.*, vol. 15, no. 10, pp. 2468–2475, Oct. 2014.

[14] L. Liu, K. Sun, X. Zhang, D. Teng, and G. Wang, "An a-IGZO TFT pixel circuit with improved current mirror for active matrix organic light emitting diode displays," in *Proc. 17th Int. Conf. Electron. Packag. Technol. (ICEPT)*, 2016, pp. 1235–1239.

[15] C. S. Choi *et al.*, "Blur-free outcoupling enhancement in transparent organic light emitting diodes: A nanostructure extracting surface plasmon modes," *Adv. Opt. Mater.*, vol. 1, no. 10, pp. 687–691, Oct. 2013.

[16] Y. Park, V. Choong, Y. Gao, B. R. Hsieh, and C. W. Tang, "Work function of indium tin oxide transparent conductor measured by photoelectron spectroscopy," *Appl. Phys. Lett.*, vol. 68, no. 19, p. 2699, 1996.

[17] Y. Guo and J. Robertson, "Origin of the high work function and high conductivity of MoO_3," *Appl. Phys. Lett.*, vol. 105, no. 22, p. 222110, Dec. 2014.

[18] Y. C. Han, M. S. Lim, J. H. Park, and K. C. Choi, "Optical effect of surface morphology of Ag on multilayer electrode applications for OLEDs," *IEEE Electron Device Lett.*, vol. 35, no. 2, pp. 238–240, Feb. 2014.

[19] Y. C. Han, M. S. Lim, J. H. Park, and K. C. Choi, "ITO-free flexible organic light-emitting diode using ZnS/Ag/MoO_3 anode incorporating a quasi-perfect Ag thin film," *Organic Electron.*, vol. 14, no. 12, pp. 3437–3443, Dec. 2013.

[20] S.-M. Lee, C. S. Choi, K. C. Choi, and H.-C. Lee, "Low resistive transparent and flexible ZnO/Ag/ZnO/Ag/WO_3 electrode for organic light-emitting diodes," *Organic Electron.*, vol. 13, no. 9, pp. 1654–1659, Sep. 2012.

[21] H. Cho, C. Yun, J.-W. Park, and S. Yoo, "Highly flexible organic light-emitting diodes based on ZnS/Ag/WO_3 multilayer transparent electrodes," *Organic Electron.*, vol. 10, no. 6, pp. 1163–1169, Sep. 2009.

[22] H.-W. Wu, R.-Y. Yang, C.-M. Hsiung, and C.-H. Chu, "Influence of Ag thickness of aluminum-doped ZnO/Ag/aluminum-doped ZnO thin films," *Thin Solid Films*, vol. 520, no. 24, pp. 7147–7152, Oct. 2012.

[23] G. Haacke, "New figure of merit for transparent conductors," *J. Appl. Phys.*, vol. 47, no. 9, p. 4086, 1976.

Authors' photographs and biographies not available at the time of publication.